High-Resolution Time-Resolved Extreme Ultraviolet Spectroscopy on NSTX

J. K. Lepson[1], P. Beiersdorfer[1,2], J. Clementson[2], M. Bitter[3], K. Hill[3], R. Kaita[3], L. Roquemore[3], C. H. Skinner[3], G. Zimmer[3]

[1] Space Sciences Laboratory, Berkeley CA 94720 [2] Lawrence Livermore National Laboratory, Livermore CA 94550 [3] Princeton Plasma Physics Laboratory, Princeton, NJ 08540

lepson@ssl.berkeley.edu

Summary:

We report here on high-resolution, time-resolved spectroscopy in the extreme ultraviolet spectral region (10-200 Å) on the NSTX tokamak. This work utilizes two flat-field spectrometers on loan from LLNL's electron beam ion trap facility.

XEUS (the X-ray and Extreme Ultraviolet Spectrometer) was installed in 2004. It has a 2400 line/mm flat-field grating with a field of view of ~50 Å that can be positioned to survey between 5 - 135 Å. XEUS has an instrumental resolution of ~0.1 Å and $\lambda/\Delta\lambda$ ~ 100 at 10 Å to ~ 1000 at 100 Å (Beiersdorfer et al. 2004).

LoWEUS (the Long-Wavelength Extreme Ultraviolet Spectrometer), installed in 2008, utilizes a 1200 line/mm flat-field grating with a field of view of ~180 Å. It is typically positioned to survey between 60-280 Å and has an instrumental resolution of ~0.3 Å and $\lambda/\Delta\lambda$ ~ 300 at 100 Å to ~ 600 at 200 Å (Lepson et al. 2010).

Wavelength calibrations were performed using well known helium-like and hydrogenic emissions of lithium, boron, carbon, nitrogen, and oxygen.

New CCD cameras have achieved a time resolution of 12-13 ms for both instruments. We are now able to examine the time dependence and evolution of both intrinsic and extrinsic impurities in the extreme ultraviolet spectral band of the NSTX plasma. Of particular interest will be monitoring the entry of molybdenum into the plasma after installation of Mo tiles during the NSTX upgrade. Unfortunately, an arc in the machine caused enough damage to cancel the run and dashed any hope of acquiring spectra this year.

We present spectra showing the charge balance evolution of M-shell metal impurities and how emissions of impurities are affected by plasma conditions.

References:

P. Beiersdorfer, E. W. Magee, E. Träbert, H. Chen, J. K. Lepson, M.-F. Gu, & M. Schmidt. *Rev. Sci. Instrum.* 75, 3723 (2004).

J. K. Lepson, P. Beiersdorfer, J. Clementson, M. F. Gu, M. Bitter, L. Roquemore, R. Kaita, P. G. Cox, & A. S. Safronova. *J. Phys. B*. 43, 144018 (2010).

Acknowledgments:

This work was supported by the DOE General Plasma Science program. Part of this work was performed under the auspices of DOE by LLNL under contract DE-AC52- 07NA27344 and PPPL under contract DE-AC02-09CH11466.

Fig. 1: XEUS and LoWEUS
(left) XEUS in place on NSTX; detector is located behind the white lead sheet to help protect it from hard x rays produced by the neutral beam source located just to the left. (right) LoWEUS in place on NSTX, located on the opposite side of the vessel from XEUS and the neutral beam injector.

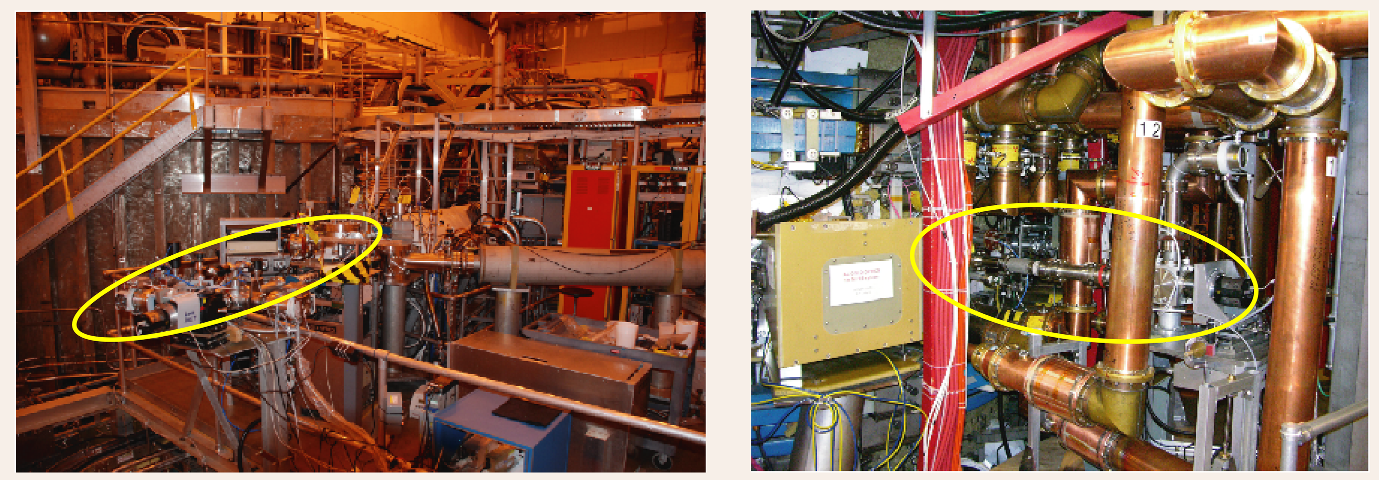

Fig. 2: XEUS calibration
Single frame (~12.5 ms duration) from XEUS spectrometer showing calibration lines of He- and H-like oxygen, nitrogen, carbon, and boron.

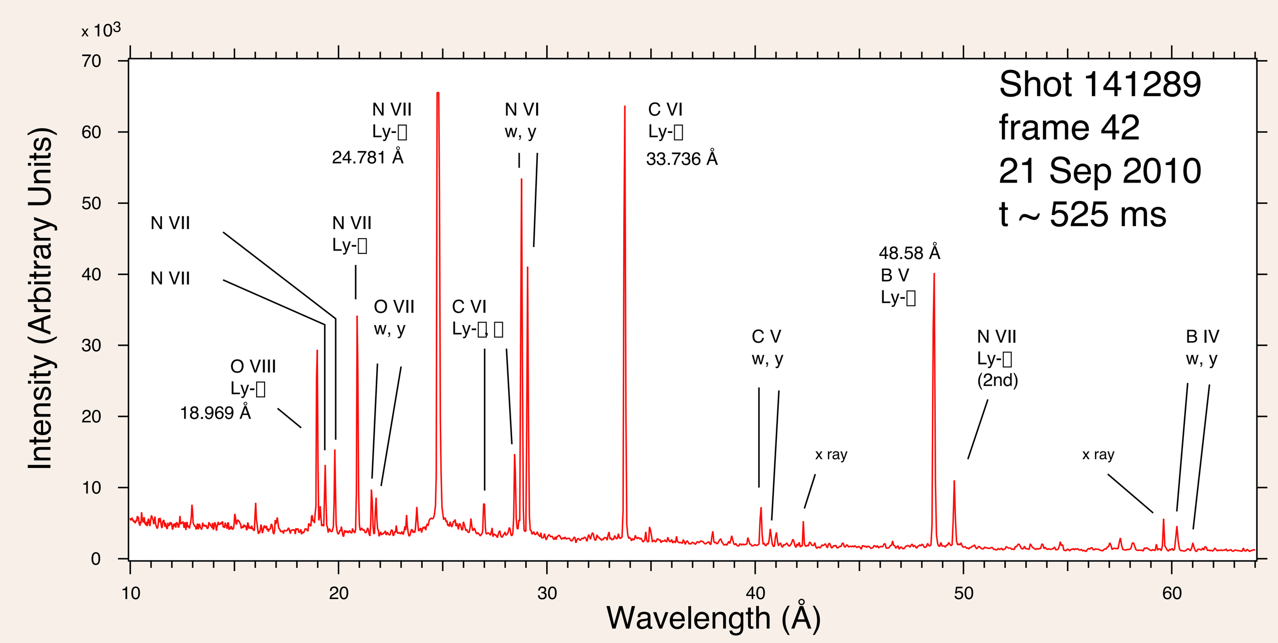

Fig. 3: LoWEUS calibration
Single frame (~12.5 ms) from LoWEUS spectrometer showing calibration lines of He- and H-like carbon and lithium.

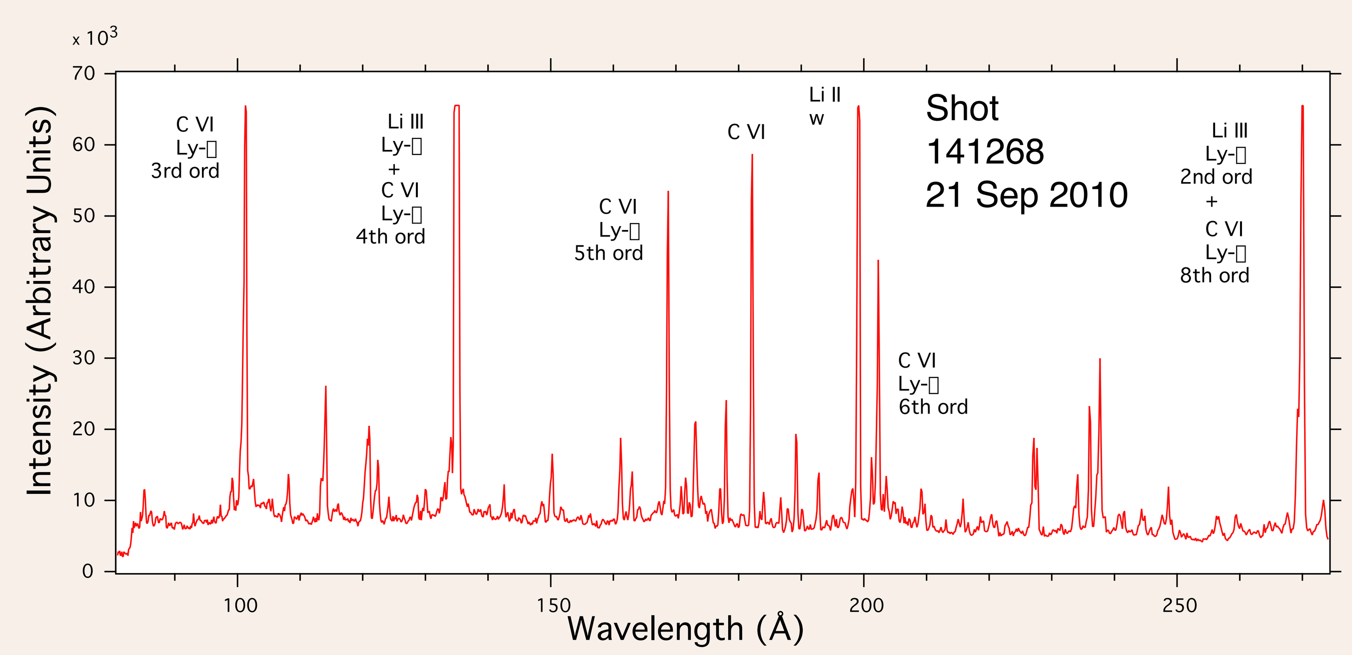

Fig. 4: Metal M-shell emission seen by LoWEUS
Single frame (~12.5 ms) from LoWEUS spectrometer showing strong emission of nickel and iron M-shell ions.

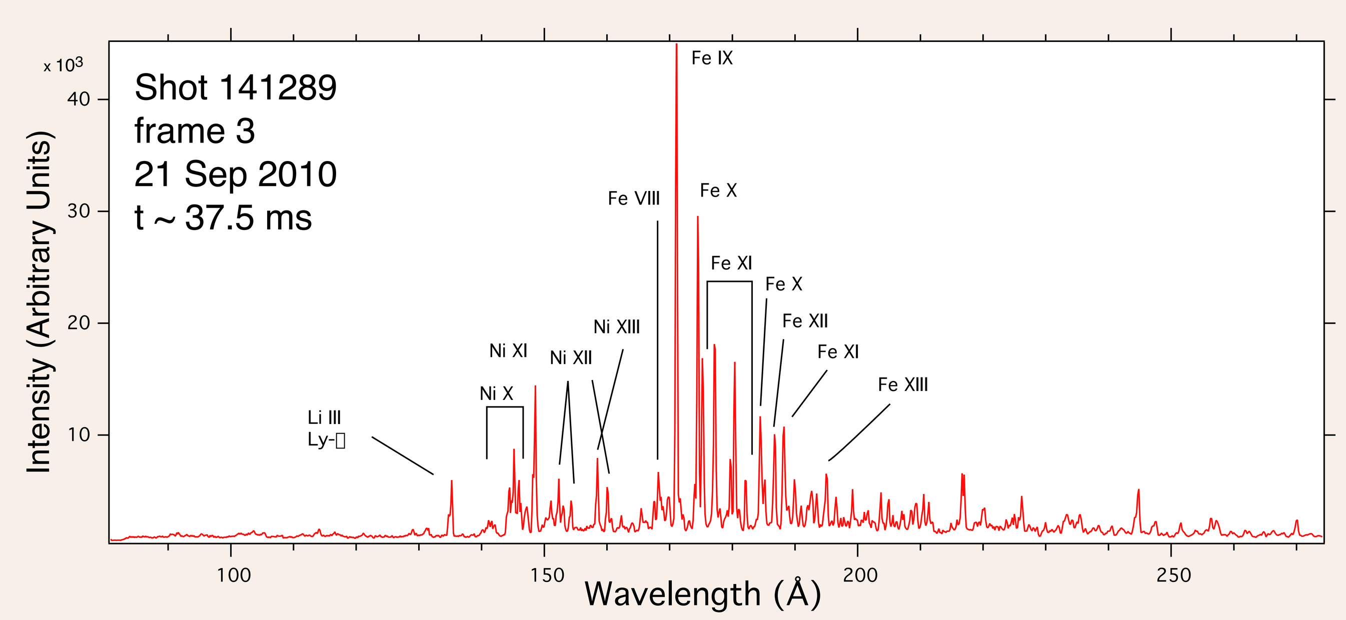

Fig. 5 Time evolution of iron impurities with XEUS spectrometer on NSTX.
(a) Image of shot 141249 with Multipoint Thomson Scattering data for temperature, density, beam current, and neutral beam injection. Emission of iron L-shell increases dramatically in conjunction with the drop in T_e just before the end of the shot.
(b) Individual frames covering the last 175 ms of shot, showing the increase in iron L-shell emission.

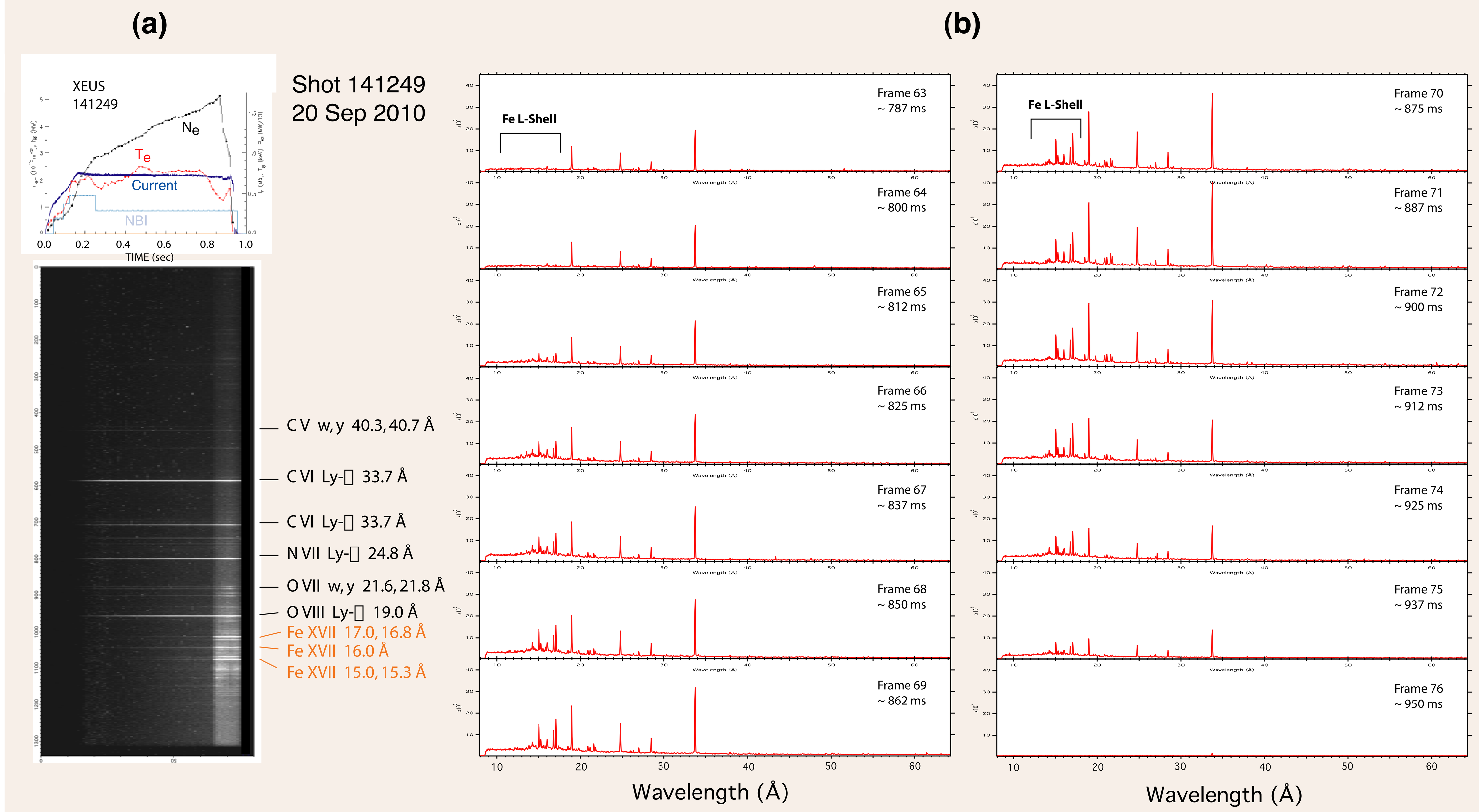

Fig. 6: Time evolution of metal impurities with LoWEUS spectrometer on NSTX.
(a) Image of shot 141224 with Multipoint Thomson Scattering data for temperature, density, beam current, and neutral beam injection. Emission of iron and nickel M-shell occurs before the plasma is heated by the neutral beam injection. Evolution of charge balance can be seen in the diagonal appearance of the lines. The image also gives a visual representation of plasma conditions: emissions, including that of iron L-shell ions, increase dramatically in conjunction with the start of neutral beam injection and also with the the drops in T_e, likely associated with edge-localized modes (ELMs), before the shot is disrupted.
(b) Individual frames covering the first 91 ms of shot, showing the appearance and burn-out of iron and nickel M-shell emission. The evolution in iron charge balance from lower charge states (Fe IX-X at 170-180 Å) to higher charge states (Fe XII-XIII at 200-225 Å) during the first 65 ms of the shot is noticeable.